Science Advances

AAAS

advances.sciencemag.org/cgi/content/full/2/5/e1600134/DC1

Supplementary Materials for

Rapid oxygenation of Earth's atmosphere 2.33 billion years ago

Genming Luo, Shuhei Ono, Nicolas J. Beukes, David T. Wang, Shucheng Xie, Roger E. Summons

Published 13 May 2016, *Sci. Adv.* **2**, e1600134 (2016)
DOI: 10.1126/sciadv.1600134

The PDF file includes:

Supplementary Materials

Geological background

The three diamond drill cores, EBA-2, EBA-4 and KEA-4, intersect well-preserved, low-grade metamorphic sedimentary strata of the late Neoarchean to early Paleoproterozoic of the Transvaal Supergoup near Carltonville in South Africa (fig. S1). The studied interval contains the Rooihoogte Formation and the base of the Timeball Hill Formation. The Rooihoogte succession is generally correlated with the Duitschland Formation cropping out in the Duitschland area (*52*) (see Rasmussen et al. (*41*) for a different correlation which puts the Rooihoogte Formation above the Duitschland Formation) which is very well constrained, not only by the presence of the sequence boundary at the base of a sharp-based quartzite unit in core EBA-4 and KEA-4, but also by the presence of the lower Duitschland glaciogenic diamictite in core EBA-4 (see below) at Carltonville and the basal Bevetts conglomerate below that (Fig. 2). Another factor in support of this correlation is the presence of thin microbial laminated carbonate beds in the uppermost part of the Rooihoogte Formation in the Carltonville area that can be broadly correlated with carbonate beds in the uppermost Duitschland Formation (Fig. 2). For detailed strata correlation in this area, the readers are referred to Coetzee (*52*), Bekker et al. (*75*), Summer and Beukes (*76*), Guo et al. (*34*) and Hoffman (*77*).

Like the Duitschland Formation, the Rooihoogte Formation, unconformably overlying the Malmani dolomite, can be divided into upper and lower Rooihoogte Formation with the sequence boundary located at ~567.5 m, ~1345.6 m and ~1089.0 m in KEA-4, EBA-2 and EBA-4 cores, respectively (Fig. 2). In all the three cores, the lower Rooihoogte Formation (below the sequence boundary) is characterized by large chert breccia, identified as the Giant Chert Breccia Member. These breccias are *in situ* karst breccia, consisting of brecciated dolomite and chert with some black shale from the late Archean Malmani dolomite. The Giant Chert Breccia Member postdates the Penge Iron Formation, which outcrop in the northeastern Transvaal basin (fig. S1). Above the Giant Chert Breccia Member is

the Bevetts Member in the KEA-4 and EBA-2 cores and diamictite in core EBA-4 (Fig. 2). The Bevetts Member developed during flooding of the erosion surface and deposition of a sheetlike basal conglomerate or poorly sorted reworked chert breccia with some black shale. The diamictite in core EBA-4 is characterized by grey muddy matrix and is correlative to the lower Duitschland diamictite in the Duitschland area. The Bevetts Member in this core has been removed during emplacement of the diamictite, which now directly contacts the Giant Chert Breccia.

The upper Rooihoogte Formation (above the sequence boundary) has a similar lithology in all the three cores, consisting of mudstone, black shale and siltstone with few chertified microbialites in the upper part and quartzite and conglomerate in the lower part (Fig. 2). Conglomerate and quartzites, characteristic sedimentary facies above the sequence boundary, are present in core KEA-4 and EBA-4, representing the lower part of the upper sequence. Core EBA-2 was drilled on a paleohigh so that the shales that overlie the quartzite unit at base of the upper Rooihoogte Fm. directly contact the Bevetts Mbr. In these cores, the sequence boundary (erosional surface) at base of the upper Rooihoogte Fm. has eroded the original iron-rich sediment above the diamictite and sits right in contact with the diamictite or Bevetts Member.

The lower part of the Timeball hill Formation is characterized by black shale with high contents of organic carbon and pyrite. Re–Os dating of synsedimentary to early diagenetic pyrite from carbonaceous shale (core EBA-2) that straddles the boundary between the Rooihoogte and Timeball Hill Formations provides a precise isochron age of 2316±7 Ma (*40*), which is supported by tuff zircon U-Pb dating of 2309±9 Ma from the lower Timeball Hill Formation (*41*). Sequence stratigraphic analysis suggested that the sequence from the upper Rooihoogte Formation to the lower part of the Timeball Formation represents continuous deposition above the unconformity over Bevetts member of the lower Rooihoogte Formation (*49*) (Fig. 1).

Potential of sulfur MIF signals originated from weathering of preexisting S-MIF

Farquhar and Wing (*25*) noted the small but significant S-MIF signals ($\Delta^{33}S < +0.5$ ‰) for the rocks deposited between 2.45 and 2.0 Ga, and called Stage II of S-MIF record. They proposed that these relatively small signals might be derived from oxidative weathering of preexisting continental sulfide and sulfate with S-MIF signals, while not directly from geologically time-equivalent atmospheric reactions. Reinhard et al. (*46*) made quantitative analysis that disappearance of S-MIF signals from weathering would take as much as a few 100s of million years, corresponding to the residence time of sulfide and sulfate minerals in continental crust. Thus, in this recycling hypothesis, non-zero pyrite $\Delta^{33}S$ values can persist long after the rise in pO_2 that prevented the atmospheric origin of S-MIF signals. The prerequisite of this long lasting recycling signal is the non-zero $\Delta^{33}S$ values of average continental crust reservoirs due to selective preservation of pyrite with positive $\Delta^{33}S$ values during Archean (*25, 46*).

The $\Delta^{33}S$ values of the seawater sulfate are controlled by the flux and $\Delta^{33}S$ values of the weathering crustal sulfur (pyrite and evaporite) and volcanically emitted SO_2, and seawater sulfate reservoir size (basin size). Generally, the $\Delta^{33}S$ values of the volcanic SO_2 are close to 0‰. Thus the $\Delta^{33}S$ values of the seawater sulfate must be lower than weathering crustal sulfur. Statistic evaluation suggests that the $\Delta^{33}S$ value of the crustal sulfur would be lower than 3‰ (*46*). Therefore the $\Delta^{33}S$ values of the seawater sulfate generally must be lower than 3‰ (Fig. 1 in Reinhard et al. (*46*)). Multiple lines of observations suggest that recycling sulfur was not the main source for the S-MIF signals found in these three cores. *Firstly*, The Transvaal depository on the Kaapvaal Craton from which our samples were collected was a large basin which was about several hundred kilometers wide. Furthermore, the basin might have been connected with the Hamersley Basin on the Pilbara Carton of Western Australia (*78, 79*). These mean that the sulfate reservoir size would be large enough to buffer weathering sulfur S-MIF signals. *Secondly*, the pyrite $\Delta^{33}S$ values in this study are close to the highest one in the whole Earth history, much higher than the mean crustal values. Thus it is difficult to ascribe these high $\Delta^{33}S$ values to

recycling sulfur. *Thirdly*, in the recycling sulfur hypothesis, the sulfate in the basin would be a sort of spatially homogeneous in sulfur isotopic composition and temporally constant in short time interval. The variable and spatial and stratigraphically heterogeneous $\Delta^{33}S$ values argue against recycling sulfur as the main mechanism for the $\Delta^{33}S$ signatures. *Fourthly,* the mixing of the recycling pyrite sulfur from sedimentary rocks with typical Neoarchean $\Delta^{36}S/\Delta^{33}S$ and other sources with different $\Delta^{36}S/\Delta^{33}S$ values would produce a $\Delta^{36}S/\Delta^{33}S$ slope deviating (albeit perhaps subtly) from the Neoarchean one. Thus, the Neoarchean-like $\Delta^{36}S/\Delta^{33}S$ slopes present in the S-MIF interval (Fig. 3), which are possibly related to atmospheric composition (e.g., *26, 48*), also argue against recycling sulfur. *Lastly*, according to modeling results of the Paleoproterozoic sulfur cycle, the crustal memory of $\Delta^{33}S$ of recycled Neoarchean-like sulfur would last for 10s to 100s million years (*46*). This suggests that the distinct but relatively small $\Delta^{33}S$ values in the transitional interval were also unlikely caused by recycling sulfur as it disappeared very quickly, in 1 to 10 million years. On the other aspect, as the section studied here is a continuous sequence, it would be most unlikely that source supply changed in such a short span of time to provide "recycled" crustal (source area) sulfur signatures that would change from S-MIF to S-MDF.

Sensitivity analysis of C-O-S biogeochemical cycling model

We conducted a sensitivity analysis for the two important parameters in the sulfur cycle, the coefficient (γ) of pyrite weathering to pO_2 and the power coefficient (θ) of the sulfate reduction (pyrite burial) to pO_2 level. We changed the power coefficient (θ) by the 20%, either increase from -0.05 to -0.04 or decrease from -0.05 to -0.06, to test the sensitivity of seawater sulfate reservoir size to this parameter. A significant increase in the seawater sulfate level was still present, although the highest value of the seawater sulfate changed a little (fig. S4). Thus the power coefficient (θ) is not sensitive to our modeling results. Our modeling results are also not sensitive to the supposed coefficient (γ) as we increase the

F_{WPY} after GOE by 2 times relative to the modern value, the seawater sulfate level is still lower than 1 mM (fig. S5).

Figures

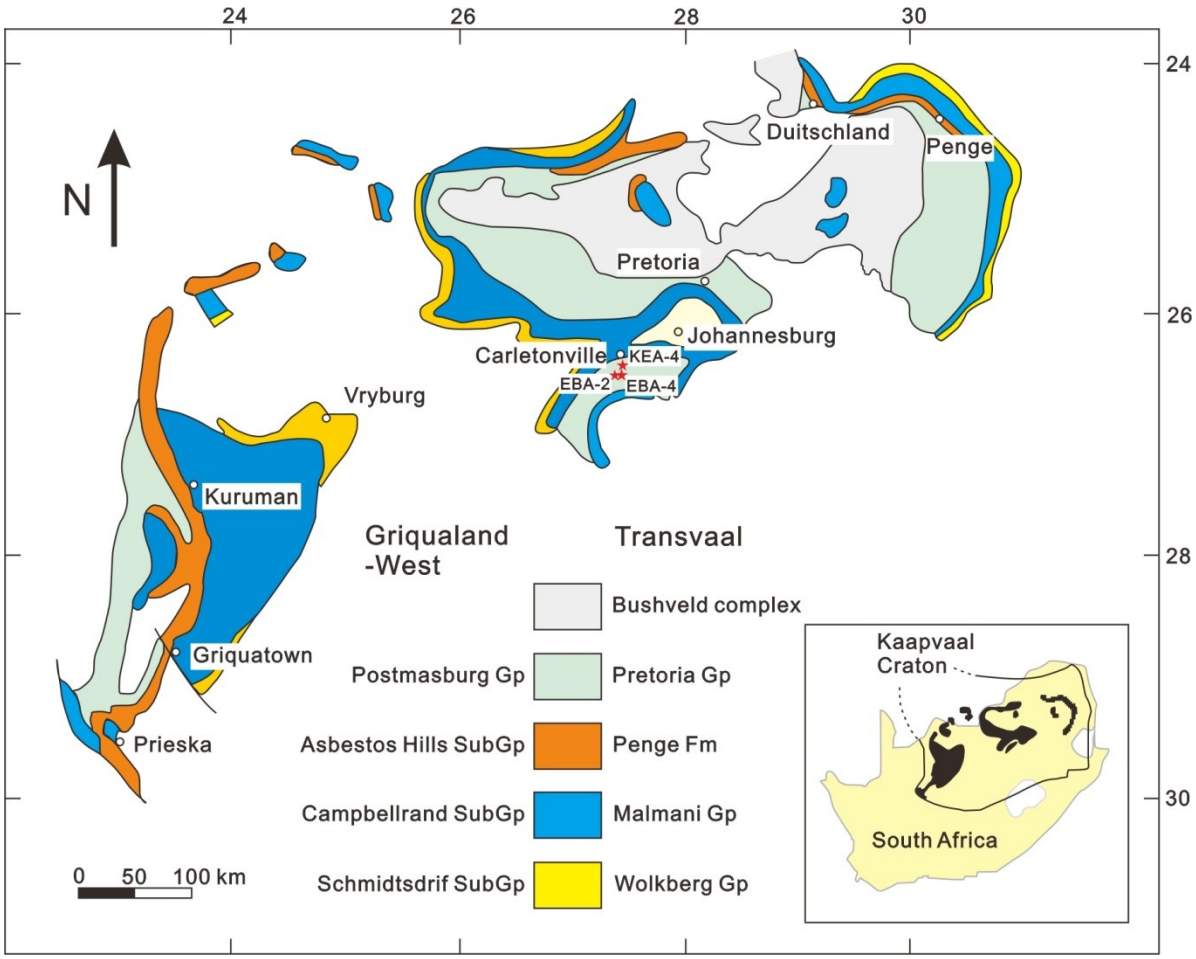

fig. S1. Simplified geological map of the Transvaal Supergroup in the Transvaal and Griqualand West basins, Kaapvaal Craton, South Africa (revised from (*76*)). Stars represent the three diamond drill cores analyzed in this study.

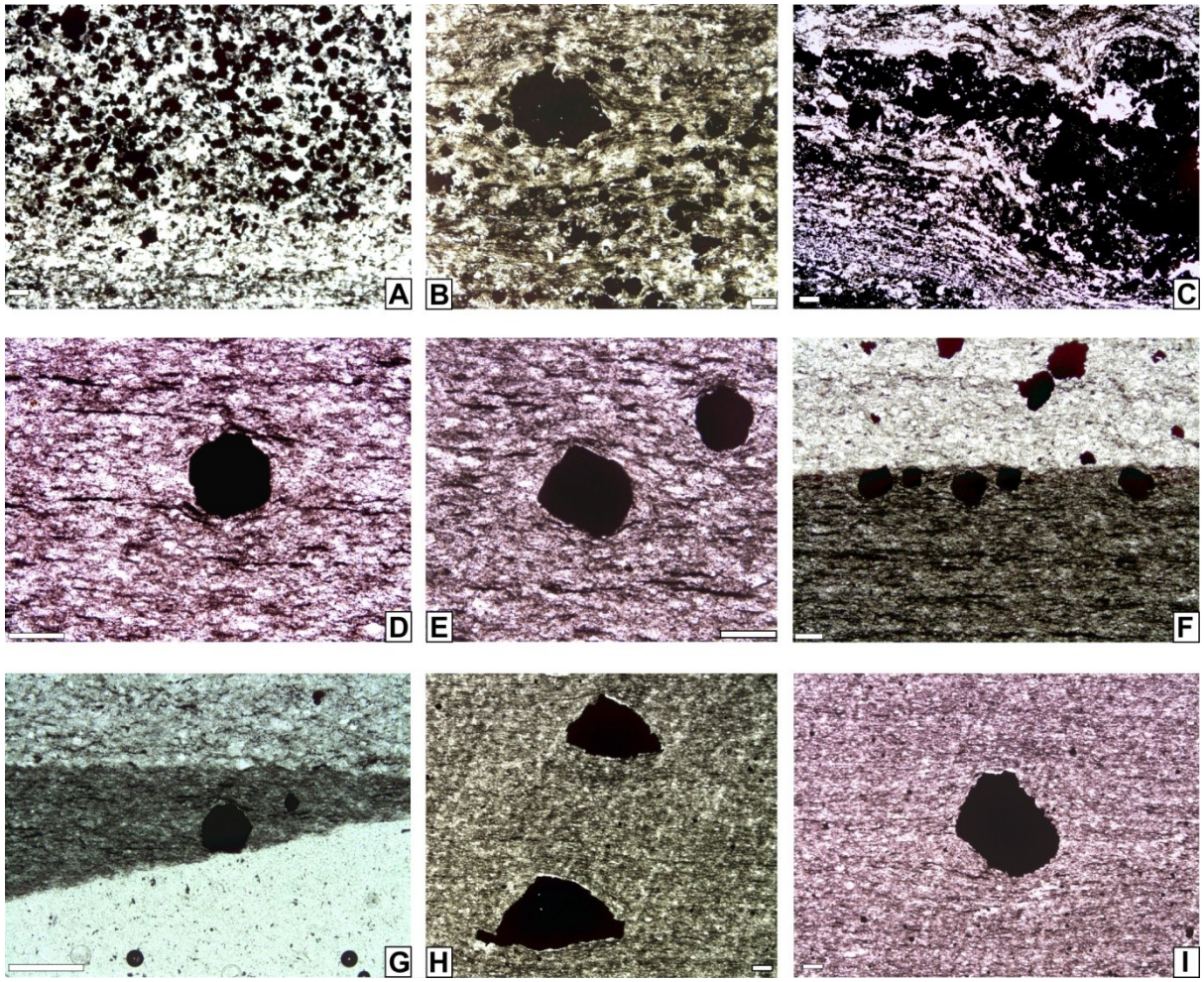

fig. S2. Representative transmitted light photomicrographs showing pyrite (opaque particles) distribution patterns in the samples analyzed in this study. The sizes of all the pyrite grains are much larger than the matrix particles. (A-C) are samples from the S-MDF interval showing disseminated pyrite particles and deformation of sedimentary lamina due to their growth. A-B, 554.38-554.56 m; C, 555.85-556.30 m. (D-I) Samples from the S-MIF interval. D to G are from 564.74-564.86 m, illustrating deformation of original sedimentary lamina (D, E and G) and size of disseminated pyrite particles do not change according to that of matrix particles (from mudstone to siltstone) (F). H and I are from 565.70-565.84 m showing deformation of original sedimentary lamina due to the growth of pyrite particles. All scale bars are 100 μm.

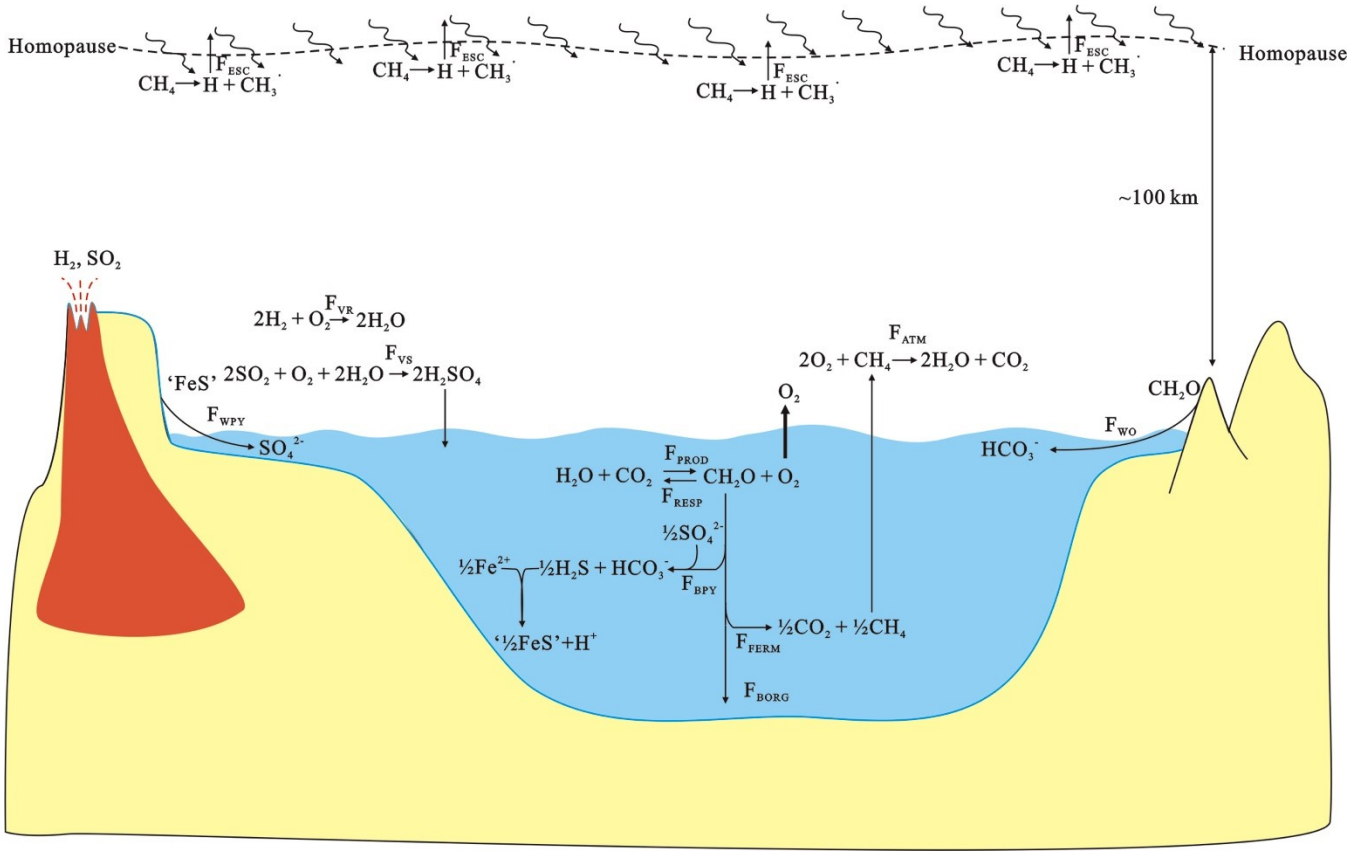

fig. S3. Cartoon figure showing the C-S-O geochemical model used in this study. 'FeS' includes both pyrite and monosulfide (e.g., pyrrhotite). Sulfate reduction to pyrite is a seven electron process but kept it to 2 for simplicity. The descriptions about the fluxes are in table S2.

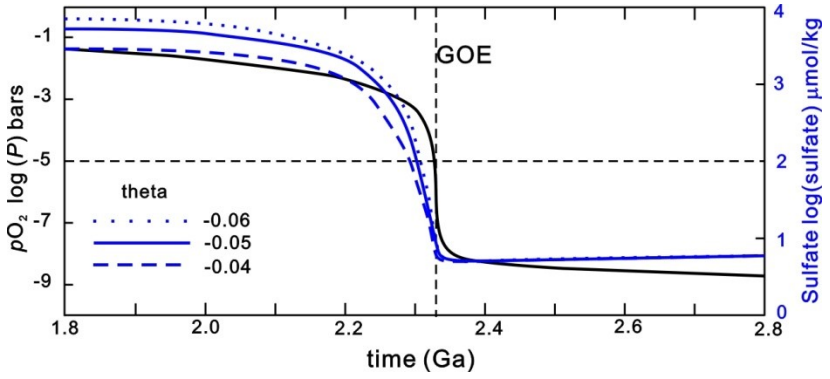

fig. S4. Sensitivity analysis for the power coefficient (θ) of pyrite burial and pO_2. θ = -0.05 is calculated from modern steady state scenario.

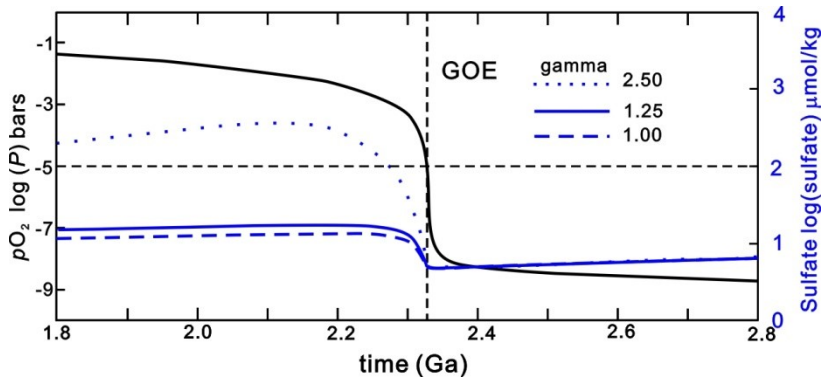

fig. S5. Sensitivity analysis for the coefficient (γ) of weathering of sulfide and pO_2. γ = 1.25 represents the weathering flux under modern pO_2.

table S1. Multiple sulfur isotope composition of the pyrite analyzed in this study. All the data are relative to VCDT.

Interval	Core	Depth (m)	$\delta^{33}S$	$\delta^{34}S$	$\delta^{36}S$	$\Delta^{33}S$	$\Delta^{36}S$	$\Delta^{36}S/\Delta^{33}S$	pyrite species
S-MDF	KEA-4	548.85	-14.6	-28.50	-54.2	0.142	-0.744	-5.3	bulk rock, mudstone
		548.85	-11.5	-22.30	-42.3	0.062	-0.334	-5.4	bulk rock, mudstone
		548.85	-14.4	-27.91	-53.2	0.106	-0.841	-7.9	Layered pyrite
		548.85	-12.8	-24.94	-47.7	0.112	-0.829	-7.4	Layered pyrite
		549.00	-15.5	-30.00	-57.2	0.100	-1.001	-10.0	Layered pyrite
		551.08	-14.4	-27.99	-53.1	0.104	-0.606	-5.8	bulk rock, mudstone
		551.08	-17.9	-34.67	-65.4	0.083	-0.609	-7.3	Layered pyrite
		551.45	-16.3	-31.51	-59.7	0.104	-0.775	-7.5	Layered pyrite
		553.40	-15.2	-29.61	-56.3	0.129	-0.850	-6.6	Layered pyrite
		553.47	-13.7	-26.54	-50.5	0.081	-0.697	-8.7	Bulk rock, mudstone
		553.47	-15.9	-30.82	-58.4	0.102	-0.728	-7.2	Layered pyrite
		553.47	-13.4	-26.10	-49.6	0.096	-0.661	-6.9	Layered pyrite
		553.47	-14.6	-28.48	-54.2	0.149	-0.806	-5.4	Layered pyrite
		553.47	-15.0	-29.09	-55.4	0.094	-0.873	-9.3	Layered pyrite
		553.47	-15.0	-29.26	-55.6	0.135	-0.802	-5.9	Layered pyrite
		553.47	-15.1	-29.27	-55.7	0.123	-0.869	-7.0	Layered pyrite
		553.47	-12.0	-23.23	-44.2	0.078	-0.522	-6.7	Layered pyrite
		553.47	-16.0	-31.07	-59.1	0.107	-0.999	-9.3	Layered pyrite
		553.47	-16.1	-31.22	-59.1	0.144	-0.713	-5.0	Layered pyrite
		553.47	-12.6	-24.73	-47.6	0.226	-1.176	-5.2	Layered pyrite
		553.47	-15.6	-30.24	-57.4	0.123	-0.792	-6.4	Layered pyrite
		553.47	-16.4	-31.87	-60.4	0.134	-0.773	-5.8	Layered pyrite
		553.92	-14.9	-29.06	-55.4	0.143	-0.980	-6.9	Layered pyrite
		553.92	-14.6	-28.41	-54.0	0.127	-0.733	-5.8	Bulk rock, mudstone
		553.92	-14.2	-27.66	-52.6	0.152	-0.785	-5.2	Bulk rock, mudstone
		553.92	-10.1	-19.99	-38.0	0.203	-0.366	-1.8	Bulk rock, siltstone
		553.92	-15.9	-30.82	-58.5	0.106	-0.767	-7.2	Layered pyrite
		554.47	-9.7	-18.82	-35.6	0.057	-0.184	-3.2	Bulk rock, mudstone
		554.47	-12.3	-24.11	-46.1	0.150	-0.808	-5.4	Layered pyrite
		555.85	-14.4	-28.10	-53.9	0.191	-1.280	-6.7	Layered pyrite
		556.10	-13.6	-26.72	-51.5	0.261	-1.387	-5.3	Bulk rock, mudstone
		556.10	-13.8	-26.87	-51.1	0.133	-0.677	-5.1	Layered pyrite
		556.10	-13.1	-25.56	-48.7	0.192	-0.781	-4.1	Layered pyrite
		556.10	-14.2	-27.58	-52.3	0.109	-0.589	-5.4	Layered pyrite
		556.85	-7.1	-13.88	-26.3	0.099	-0.061	-0.6	Bulk rock, chertified
		558.56	-11.3	-22.27	-42.4	0.225	-0.496	-2.2	Bulk rock, chertified
	EBA-2	1153.92	-15.3	-29.75	-56.3	0.095	-0.5	-5.6	Bulk rock, mudstone
		1336.33	12.6	24.61	47.4	0.014	0.1	8.1	Granular pyrite
		1336.33	-12.7	-24.74	-47.0	0.095	-0.5	-5.4	Layered pyrite
		1336.60	-16.5	-32.06	-60.7	0.121	-0.7	-6.2	Layered pyrite
		1337.28	6.2	11.98	23.0	0.057	0.1	1.9	Bulk rock, mudstone
		1337.28	6.0	11.61	22.2	0.060	0.1	1.0	Bulk rock, siltstone
		1337.28	2.4	4.55	9.2	0.017	0.6	32.5	Bulk rock, mudstone
		1338.27	-16.6	-32.22	-61.0	0.092	-0.8	-8.4	Layered pyrite
		1338.27	-3.7	-7.50	-14.2	0.126	0.0	0.1	Bulk rock, mudstone
		1338.27	-16.8	-32.55	-61.6	0.083	-0.7	-8.5	Granular pyrite
		1338.78	4.5	8.56	16.7	0.055	0.4	6.3	Bulk rock, mudstone
	EBA-4	1070.2	-16.3	-31.65	-60.2	0.140	-1.024	-7.3	Layered pyrite
		1071.21	-8.4	-16.53	-31.4	0.177	-0.226	-1.3	Bulk rock, mudstone
		1072.13	-10.1	-19.97	-38.0	0.263	-0.417	-1.6	Bulk rock, mudstone
		1072.35	-12.2	-24.10	-45.8	0.267	-0.555	-2.1	Bulk rock, mudstone

		1072.35	-15.8	-30.65	-58.1	0.133	-0.701	-5.3	Layered pyrite
		1072.82	-15.8	-30.81	-58.6	0.156	-0.897	-5.7	Layered pyrite
		1073.05	-10.3	-20.14	-38.3	0.100	-0.366	-3.7	Bulk rock, mudstone
		1073.55	-17.8	-34.52	-65.4	0.129	-0.933	-7.2	Layered pyrite
		1073.55	-18.0	-34.86	-66.4	0.135	-1.272	-9.4	Bulk rock, mudstone
		1074.38	4.6	8.79	16.8	0.107	0.067	0.6	Layered pyrite
		1075.3	6.7	12.79	25.1	0.164	0.643	3.9	Bulk rock, mudstone
		1076.25	11.9	23.14	44.5	0.025	0.102	4.1	Granular pyrite
		1076.3	5.9	11.14	21.1	0.205	-0.203	-1.0	Bulk rock, chertified
		1076.35	9.4	18.23	34.8	0.041	-0.140	-3.4	Granular pyrite
		1076.39	6.8	13.10	25.0	0.040	-0.059	-1.5	Bulk rock, siltstone
Transitional	KEA-4	559.89[&]	2.6	4.25	8.1	0.461	0.002	0.0	Bulk rock, chertified
		560.45	12.3	22.96	44.0	0.497	-0.037	-0.1	Bulk rock, chertified
		561.09	6.4	10.67	20.1	0.944	-0.242	-0.3	Layered pyrite
		561.09	4.6	6.53	12.2	1.248	-0.227	-0.2	Layered pyrite
		561.09	9.3	17.96	34.5	0.090	0.052	0.6	Bulk rock, mudstone
		561.52	8.0	14.21	26.7	0.721	-0.498	-0.7	Bulk rock, mudstone
		561.52	9.8	18.90	36.3	0.089	0.047	0.5	Bulk rock, mudstone
		561.52	10.0	19.16	36.8	0.152	0.045	0.3	Granular pyrite
		561.52	7.4	14.25	27.1	0.095	-0.112	-1.2	Granular pyrite
		562.84	8.7	16.54	31.5	0.259	-0.166	-0.6	Bulk rock, mudstone
		562.84	8.7	16.29	31.0	0.301	-0.213	-0.7	Layered pyrite
		562.84	8.7	16.89	32.3	0.085	0.004	0.0	Granular pyrite
	EBA-2	1340.88[&]	2.7	1.81	2.6	1.765	-0.8	-0.48	Bulk rock, mudstone
		1340.15	8.0	15.19	28.9	0.159	-0.1	-0.92	Bulk rock, siltstone
		1340.15	-1.0	-5.37	-10.1	1.750	0.0	0.02	Bulk rock, mudstone
		1341.77	8.2	15.81	30.2	0.071	0.0	-0.41	Bulk rock, siltstone
		1341.77 [&]	6.8	13.21	26.9	-0.025	1.6	13.20	Bulk rock, siltstone
		1341.77	8.0	14.94	28.4	0.337	-0.1	-0.40	Bulk rock, mudstone
	EBA-4	1077.94[&]	3.8	3.42	5.5	2.009	-1.029	-0.5	Bulk rock, mudstone
		1078.59[&]	2.1	0.87	2.0	1.617	0.384	0.2	Bulk rock, mudstone
		1079.8	7.8	15.01	28.7	0.079	-0.043	-0.5	Bulk rock, mudstone
		1079.8	7.3	14.03	26.7	0.123	-0.121	-1.0	Bulk rock, mudstone
S-MIF	KEA-4	563.68	8.6	4.45	2.4	6.284	-6.053	-1.0	Bulk rock, siltstone
		564.33	8.6	2.39	-2.8	7.350	-7.359	-1.0	Bulk rock, mudstone
		564.33	7.1	3.58	1.8	5.185	-4.965	-1.0	Bulk rock, siltstone
		564.33	6.0	6.40	10.0	2.739	-2.161	-0.8	Bulk rock, mudstone
		564.8[&]	8.3	8.99	13.7	3.637	-3.381	-0.9	Bulk rock, mudstone
		564.8[&]	7.5	8.75	14.4	3.002	-2.261	-0.8	Bulk rock, mudstone
		564.8	7.3	12.72	23.5	0.731	-0.838	-1.1	Granular pyrite
		564.8	8.8	9.90	15.4	3.683	-3.470	-0.9	Layered pyrite
		565.77	11.0	18.04	33.1	1.714	-1.427	-0.8	Bulk rock, mudstone
		565.77	10.5	16.91	30.8	1.811	-1.530	-0.8	Granular pyrite
		565.77	10.9	10.88	15.9	5.270	-4.772	-0.9	Layered pyrite
		565.92	9.2	13.44	23.7	2.252	-1.986	-0.9	Bulk rock, siltstone
		565.92	7.8	11.07	19.3	2.085	-1.778	-0.9	Bulk rock, mudstone
		566.08	9.4	15.41	28.2	1.449	-1.199	-0.8	Bulk rock, mudstone
		568.07	8.3	5.85	6.1	5.308	-5.014	-0.9	Granular pyrite
		568.07	7.8	10.33	17.3	2.508	-2.403	-1.0	Granular pyrite
		568.07	9.0	9.69	14.7	4.010	-3.730	-0.9	Clumpy pyrite
		570.32	8.1	14.72	27.7	0.504	-0.461	-0.9	Granular pyrite
		570.32	2.4	2.39	3.3	1.128	-1.196	-1.1	Granular pyrite
		570.32	7.0	4.48	4.0	4.680	-4.543	-1.0	Granular pyrite
		570.63	10.3	15.27	27.0	2.428	-2.129	-0.9	Granular pyrite
		570.63	14.1	25.32	47.8	1.130	-0.805	-0.7	Granular pyrite

		574.8	11.0	9.96	13.5	5.859	-5.434	-0.9	Bulk rock, mudstone
	EBA-2	1343.24	7.9	13.90	26.0	0.778	-0.532	-0.68	Bulk rock, mudstone
		1344.55	7.4	11.12	19.8	1.636	-1.364	-0.83	Bulk rock, siltstone
		1344.55	7.1	10.99	19.7	1.491	-1.305	-0.88	Bulk rock, mudstone
		1345.17	9.3	6.69	7.4	5.782	-5.305	-0.92	Bulk rock, siltstone
		1345.17	9.0	7.79	10.4	5.004	-4.425	-0.88	Bulk rock, mudstone
		1345.17	8.9	7.58	9.8	5.012	-4.570	-0.91	Bulk rock, mudstone
		1345.47	8.5	12.97	23.2	1.778	-1.507	-0.85	Bulk rock, mudstone
		1345.47	9.8	14.61	25.9	2.327	-1.980	-0.85	Bulk rock, mudstone
		1353.72[&]	8.7	8.00	11.7	4.592	-3.543	-0.77	Bulk rock, chertified
		1353.72	8.3	7.10	9.8	4.598	-3.746	-0.81	Bulk rock, chertified
	EBA-4	1080.49	5.0	6.17	10.2	1.856	-1.576	-0.8	Bulk rock, siltstone
		1080.49	5.2	8.74	16.3	0.698	-0.401	-0.6	Bulk rock, mudstone
		1080.65	5.6	7.43	12.7	1.815	-1.433	-0.8	Bulk rock, siltstone
		1080.65	6.2	10.97	20.6	0.584	-0.384	-0.7	Bulk rock, mudstone
		1082.45	9.3	8.87	12.6	4.679	-4.239	-0.9	Bulk rock, mudstone
		1082.45	13.5	24.38	46.3	0.985	-0.542	-0.6	Bulk rock, siltstone
		1083.18[&]	1.0	-1.03	-2.2	1.529	-0.216	-0.1	Bulk rock, mudstone
		1089.54	-0.5	-6.22	-14.4	2.749	-2.626	-1.0	Bulk rock, siltstone
		1089.54	9.9	6.14	5.3	6.687	-6.378	-1.0	Granular pyrite

table S2. Parameters used for Archean-Proterozoic oxygen-methane-sulfur cycle model.

Symbol	Description	Parameterization*	Note
F_{PROD}	Primary productivity	400	Approximately 1/10th of marine productivity today (*53*)
F_{RESP}	Aerobic respiration	$[O]/(3.7\times10^{5}+[O])$ (F_{PROD}-F_{BORG}-2F_{BPY})	Following Goldblatt et al. (*54*), carbon and pyrite burial terms are subtracted from organic carbon available for aerobic respiration
F_{BPY}	Pyrite burial	$3.53\ [S]/(1.4\times10^{4}+[S])\times[O]^{\theta}$	We assumed pyrite burial depends on [O] (θ) due to the change in the supply of organic material to sulfate reducers.
F_{FERM}	Flux of organics fermented to methane	from steady state for $[C_{org}]$	
F_{BORG}	Flux of organic burial	10	Holland (*2*), Claire et al. (*53*)
F_{VR}	Flux of reducing gas from volcanoes	$4.8\exp(0.45t)$	*t* is time in in Ga (giga year before present). Holland (*63*)
F_{WO}	Oxygen consumption by weathering	$8.29\times10^{-4}[O]^{0.5}$	Modified from Claire et al. (*53*)
F_{VS}	Volcanic sulfur flux	$0.0825F_{VR}$	From the present day ratio of SO_2/H_2. Holland (*63*)
F_{BGYP}	Gypsum burial	5.99×10^{-8} [S]	From modern gypsum burial rate of 2.5 Tmol S/year# and present day [S]
F_{WPY}	Oxidative pyrite weathering	$\gamma\times[O]/(3.7\times10^{4}+[O])$	Monod type kinetics (γ) for [O]#
F_{ESC}	Hydrogen Escape	3.7×10^{-5} [M]	Claire et al. (*53*)
F_{ATM}	Atmospheric methane oxidation	k_{ATM} [O][M]	k_{ATM} is derived by 4th order polynomyal fit from Fig. 3 of Claire et al. (*53*)

*, units are in Tmol and Tmol/year for concentrations and flux, respectively.
#, average S:C ratio of 1:8 in pelagic sediments (e.g., Berner and Raiswell (*80*)) gives pyrite burial rate of 1.25 Tmol/year for organic carbon burial of 10 Tmol. Sulfate burial is assumed to be twice as large as pyrite burial based upon isotope mass balance (e.g., Garrels and Lerman (*81*))